Journal of Alloys and Compounds 505 (2010) 668–674

Contents lists available at ScienceDirect

Journal of Alloys and Compounds

journal homepage: www.elsevier.com/locate/jallcom

Effect of La-substitution on the structure and dielectric properties of $BaBi_4Ti_4O_{15}$ ceramics

A. Chakrabarti, J. Bera*

Department of Ceramic Engineering, National Institute of Technology, Rourkela 769008 Orissa, India

ARTICLE INFO

Article history:
Received 12 April 2010
Received in revised form 8 June 2010
Accepted 12 June 2010
Available online 25 June 2010

Keywords:
Ceramics
Ferroelectrics
Precipitation
Dielectric response
X-ray methods

ABSTRACT

Four-layer Aurivillius compound $BaBi_{4-x}La_xTi_4O_{15}$ ($x = 0.1–1.0$) is synthesized by a modified chemical route. X-ray diffraction analysis confirms the formation of single-phase Aurivillius compound. The crystal structure of compound changes from orthorhombic to pseudo-tetragonal at $x = 0.5$. $BaBi_{4-x}La_xTi_4O_{15}$ shows typical relaxor behaviour. With increasing La^{3+} substitution, shift of T_m towards lower temperature and increased relaxor behaviour is observed. The substitution also results in a marked improvement in the remnant polarization and coercive field. The Cole–Cole plots show the presence of two semicircular arcs, suggesting the existence of grain and grain-boundary effects. The dc-conductivity and activation energies for both grain and grain boundary are evaluated. The ceramics with $x = 0.3$ presents the lowest conductivity among all compositions.

1. Introduction

$BaBi_4Ti_4O_{15}$ (BBT) belongs to the family of bismuth layer-structured ferroelectrics (BLSFs). In recent years, BLSFs have gained significant importance for application in (non-volatile) ferroelectric random access memory (FRAM) due to their fatigue-free nature [1,2]. They are also technologically important for application in actuators, electro-optical and high temperature piezoelectric devices [3–5].

The structure of BLSFs are generalized by $(Bi_2O_2)^{2+}(A_{m-1}B_mO_{3m-1})^{2-}$, where A is relatively large size divalent or trivalent cation in 12-coordination site, B is small size, highly charged cation in octahedral coordination site of pseudo-perovskite unit and m indicates the number of oxygen octrahedral units stacked along the c-axis between $(Bi_2O_2)^{2+}$ layers [6]. Normally, the polarization of BLSFs is along the a-axis and is attributed to the displacement of A-site cations [7,8]. The sintering of BLSFs at a high temperature, results in the volatilization of bismuth. The bismuth volatilizations lead to the formation of oxygen vacancies in order to maintain the charge neutrality. These oxygen vacancies are responsible for their conductivity. In order to minimize the drawback, as well as to tailor the ferroelectric properties of BLSFs, many studies have been concentrated on its A and/or B-site substitutions [9–15].

La^{3+} substitution plays an effective role in improving properties of many BLSFs [13,16–19], especially of $Bi_4Ti_3O_{12}$ [20,21]. La^{3+} substitution for Bi^{3+} results in a transition from ferroelectric to relaxor behaviour in $SrBi_4Ti_4O_{15}$ and $Bi_4Ti_3O_{12}$ [9,19,21]. The substitution is also helpful in increasing remnant polarization and decreasing coercive field of many BLSFs [9,22–24]. Concentration of Bi ion vacancies and oxygen vacancies is reported to decrease by La^{3+} substitution [25]. This may be due to the reason that as the metallicity of La^{3+} is stronger and also more stable in comparison to that of Bi^{3+}, probably the oxygen ions near La^{3+} are more stable than those near Bi^{3+}. Thus the generation of oxygen vacancies is restrained by the substitution of La^{3+} for Bi^{3+}. As a result, the dc-conductivity of these compounds also decreases. Incorporation of La changes the orthorhombic crystal structure of $Bi_{4-x}La_xTi_3O_{12}$ to tetragonal at $x \geq 1.0$ [26]. All these indicate that the substitution has multi-faced effect in BLSFs.

Present work reports the synthesis and characterization of La^{3+} substituted $BaBi_{4-x}La_xTi_4O_{15}$ ceramics. Among the four-layer BLSFs, BBT is one of the relaxor ferroelectric material which has lead free composition [9,27]. La^{3+} may be a potential substituent for improving the relaxor and ferroelectric behaviour in BBT ceramics. However, no reports regarding the substitution in BBT is available in the literature to the best of author's knowledge.

2. Experimental

$BaBi_{(4-x)}La_xTi_4O_{15}$ ceramics with $x = 0.1$, 0.2, 0.3, 0.5, 1.0 compositions (denoted as BBLT1, BBLT2, BBLT3, BBLT5 and BBLT10, respectively) were synthesized through a cost-effective chemical method [27]. Barium nitrate $Ba(NO_3)_2$ (Merck India Ltd., Assay >99%), bismuth nitrate $Bi_2(NO_3)_3.5H_2O$ (Merck India Ltd., Assay >99%), tita-

* Corresponding author. Tel.: +91 0661 2462201.
E-mail addresses: jbera@nitrkl.ac.in, jbera@rediffmail.com (J. Bera).

0925-8388/$ – see front matter © 2010 Elsevier B.V. All rights reserved.
doi:10.1016/j.jallcom.2010.06.105

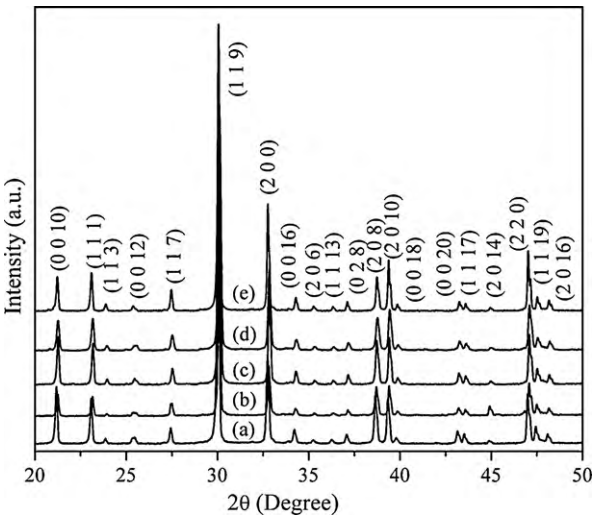

Fig. 1. XRD pattern of $BaBi_{(4-x)}La_xTi_4O_{15}$ ceramics (a) $x = 0.1$, (b) 0.2, (c) 0.3, (d) 0.5, (e) 1.0.

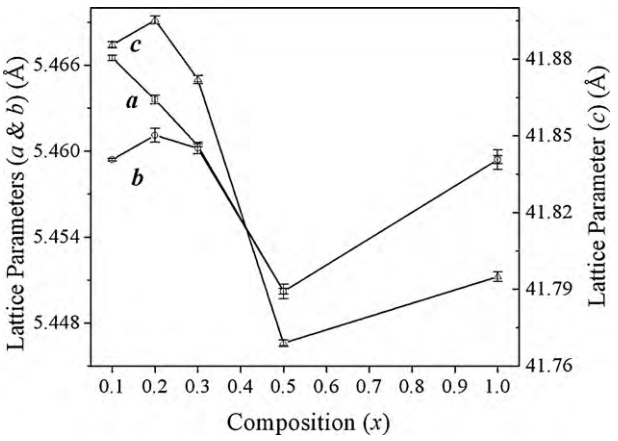

Fig. 2. Lattice parameters of $BaBi_{4-x}La_xTi_4O_{15}$ ceramics as a function of La^{3+} concentration (x).

nium dioxide TiO_2 (Merck India Ltd., Assay >99%, particle size: $d_{10} = 0.27$ μm, $d_{50} = 0.35$ μm, $d_{90} = 0.48$ μm), La_2O_3 (Merck India Ltd., Assay >99%) and oxalic acid $(COOH)_2{\cdot}2H_2O$ (Merck India Ltd., Assay >99%) were used as raw materials. Required amount of bismuth nitrate and lanthanum oxide were dissolved in minimum quantity of concentrated nitric acid. This solution was added into barium nitrate aqueous solution to form a clear Bi,-Ba,-La-nitrate solution. The mixed solution thus obtained was added drop-wise into TiO_2-oxalic acid suspension under vigorous stirring. Barium, bismuth and lanthanum oxalates were precipitated on the surface of TiO_2 particles during the addition. Finally suspension was aged for 24 h after adjusting the pH of it to 7. The precipitate was then separated by filtration and dried.

The powder precursor was repeatedly calcined at 800, 950 and 1000 °C with intermediate grindings. Calcined powders were ground and uniaxially pressed into circular shaped discs at a pressure of 220 MPa using polyvinyl alcohol as binder. The pellets were sintered in the temperature range 1100–1145 °C depending on the composition. Densities of sintered samples were measured by Archimedes principle. The pellets having more than 96% of theoretical density were used for further characterization.

The phase formation during calcination steps was investigated by powder X-ray diffraction (XRD) analysis using Cu Kα radiation (PW-1830, Philips, Netherlands. The microstructures of sintered specimens were studied using scanning electron microscope (SEM) (JSM-6480LV). For dielectric and impedance measurements, the sintered pellets were electroded with silver conductive paste (Alfa Aesar) and cured at 600 °C for 30 mins. The dielectric constant and loss factor were measured using an Impedance Analyzer (Solatron 1260) in the range from room temperature to 550 °C with a heating rate of 1 °C min^{-1} and in the frequency range of 1 Hz to 5 MHz. The ferroelectric hysteresis loop measurement was performed in a *P–E* loop tracer (Radiant Technologies).

3. Results and discussion

3.1. XRD Analysis

Fig. 1 shows the X-ray diffraction patterns of $BaBi_{(4-x)}La_xTi_4O_{15}$ ceramics. Diffraction patterns of all compositions matched with standard $BaBi_4Ti_4O_{15}$ phase (JCPDS Card No. 35-0757). No other secondary phase is detected. So La^{3+} shows complete solid solution formation in BBT for the composition range $x \leq 1.0$. The strongest diffraction peak (1 1 9) is consistent with the (1 1 2m + 1) highest diffraction peak for Aurivillius phase [28]. Lattice parameters are evaluated through Rietveld analysis using MAUD [29] program considering orthorhombic $A2_1am$ space group. Fig. 2 shows the change in lattice parameter with lanthanum substitution (x). All three lattice parameters decrease nominally up to $x = 0.5$. This may be due to the occupancy of La in pseudo-perovskite layer and associated changes in Ti-O_6 octahedral tilting in the unit cell [30,31]. A slight increase in lattice parameters near $x = 1.0$, may be due to the occupancy of La^{3+} in Bi_2O_2 layer over and above perovskite layer occupancy. It has been found through Raman studies [17] that the La^{3+} begins to occupy the Bi-site in Bi_2O_2 layers of $Bi_{3-x}La_xTiNbO_9$ when $x > 0.50$. The figure also shows the change of orthorhombic structure to pseudo-tetragonal around $x = 0.5$.

It is also observed that the degree of a-axis orientation (α) increases with increasing La^{3+} content. α can be represented [32]:

$$\alpha = \frac{I(2\,0\,0)}{[I(2\,0\,0) + I(1\,1\,9)]}, \quad (1)$$

where I(1 1 9) and I(2 0 0) denote the XRD intensities of (1 1 9) and (2 0 0) reflections. The α values are 0.21, 0.24, 0.25, 0.26, and 0.27, respectively for composition serially from BBLT1 to BBLT10. This increasing trend of α could be explained by the fact that the crystal structure changes from orthorhombic to tetragonal.

3.2. Microstructure

Fig. 3 shows the SEM micrograph of BBLT1 and BBLT5 ceramics. Ceramics are composed of randomly oriented plate-like grains. The length and breadth of the grains are much larger compared to its thickness due to the preferred growth of grains along the plane perpendicular to the c-axis. As BLSFs crystals possess lower surface energy along {0 0 1} plane, it results crystal growth in a–b plane during sintering attaining a plate-like morphology [25]. With increase in substitution, the plate-like grains show a transformation towards circular shaped grains with rounded edges. The figure also shows the decrease of grain size in BBLT5 compared to BBLT1. So La^{3+} ion acts as a grain growth inhibitor.

3.3. Dielectric and diffuse phase transition behaviour

Fig. 4 displays the temperature dependence of dielectric constant (ε') and dielectric loss (tan δ) of $BaBi_{(4-x)}La_xTi_4O_{15}$ ceramics. Maximum dielectric constant (ε_m'), dielectric maxima temperature (T_m) and room temperature dielectric constant (ε_{RM}) are shown in Table 1. It is noted that ε_{RM} increases with increasing substitution, which is due to the shifting of ε_m' peak towards room temperature. However, ε_m' decreases with increasing substitution. This may be due to the decrease in lattice parameter 'a' and associated relaxation in structural distortion. Smaller the lattice parameter, lower will be polarization as ferroelectricity in BLSFs arises by the A-type cation displacement along 'a' direction [18,33].

Dielectric dispersion is more pronounced in tan δ versus temperature plots shown in Fig. 4(b). The loss decreases with increasing substitution. In general, oxygen vacancies are responsible for the

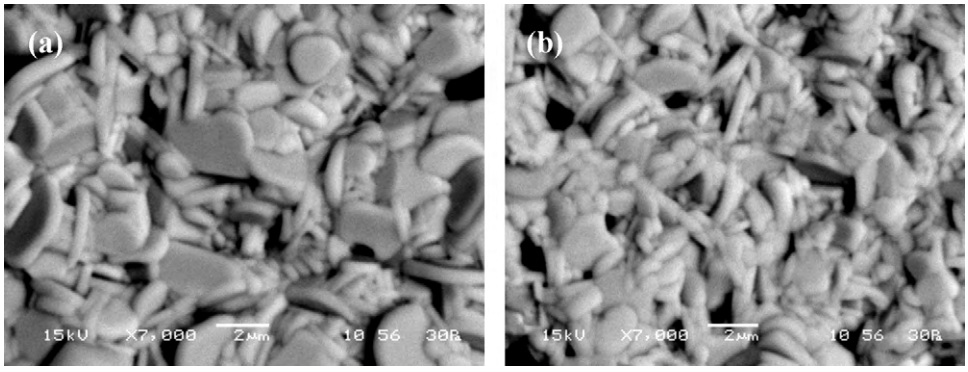

Fig. 3. Scanning electron micrograph of $BaBi_{4-x}La_xTi_4O_{15}$ ceramics (a) $x = 0.1$ and (b) $x = 1.0$.

Table 1
Room temperature relative permittivity (ε_{RM}), maximum relative permittivity (ε'_m), maximum permittivity temperature (T_m), degree of diffuseness (δ) at 100 kHz and degree of frequency dispersion (ΔT_m), fitting parameters from Vogel–Fulcher relation (E_a, T_f and ν_0), Remnant polarization ($2P_r$) and Coercive field ($2E_c$) values for different $BaBi_{(4-x)}La_xTi_4O_{15}$ ceramics.

Formula	BBLT1	BBLT2	BBLT3	BBLT5	BBLT10
ε_{RM}	270	356	366	411	221
ε_m'	2102	1697	1227	780	–
T_m (°C)	370	330	290	200	–
ΔT_m (°C)	20	30	40	50	–
δ (°C)	158 (1)	196 (1)	232 (2)	280 (3)	–
E_a (eV)	0.067 (1)	0.066 (3)	0.098 (2)	1.002 (3)	–
T_f (°C)	310	307	177	100	–
ν_0 ($\times 10^{10}$ Hz)	3.34	9.91	1.08	1.18	–
$2P_r$ ($\mu C\,cm^{-2}$)	0.295	0.61	0.834	0.556	0.055
$2E_c$ ($kV\,cm^{-1}$)	8.35	9.87	9.53	8.08	0.37

dielectric losses in BLSFs [34]. La^{3+} is substituted for volatile Bi^{3+}. So the substitution suppresses the formation of A-site as well as oxygen vacancies. This eventually leads to a decreased dielectric loss with substitution.

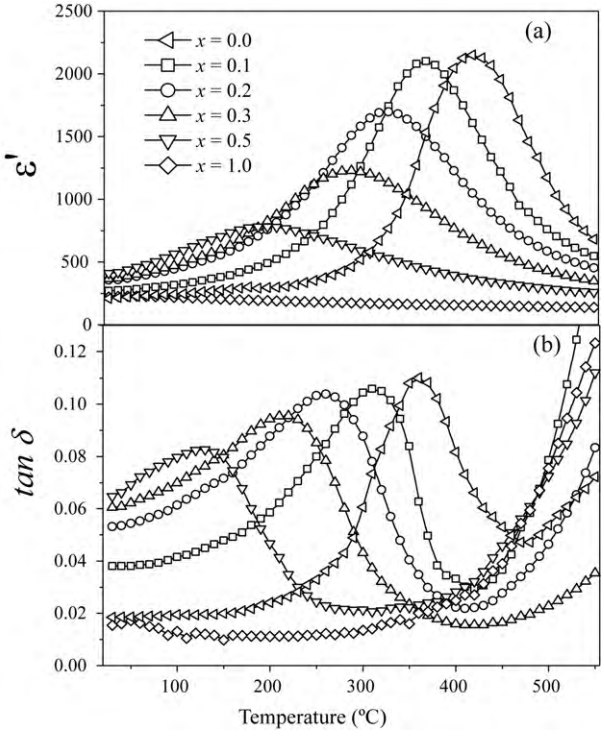

Fig. 4. Temperature dependence of ε' and $\tan\delta$ for $BaBi_{(4-x)}La_xTi_4O_{15}$ ceramics ($x = 0.1, 0.2, 0.3, 0.5, 1.0$) at 100 kHz.

T_m shifts to lower temperatures with La^{3+} substitution. This is due to the increase in size of A-site cation [35]. Further, the decrease of T_m can be explained on the basis of tolerance factor t given by:

$$t = \frac{R_A + R_B}{\sqrt{2(R_B + R_O)}} \quad (2)$$

where R_A, R_B and R_O are the effective ionic radii for A-site, B-site and oxygen ion, respectively. As the tolerance factor t increases, the structural distortion and hence the Curie temperature decreases [36]. The ionic radius of La^{3+} is larger than that of Bi^{3+}. So, the substitution will increase the tolerance factor and T_m will decrease.

All compositions exhibit a broad permittivity maximum with temperature. The broadness increases with increasing substitution rate. Peak broadening may be quantified by the parameter δ, which is related with permittivity and temperature as follows [37]:

$$\frac{1}{\varepsilon'} - \frac{1}{\varepsilon_{m'}} = \frac{(T - T_m)^2}{2\varepsilon_m \delta^2} \quad (3)$$

δ parameters of different compositions are calculated by fitting permittivity-temperature data and are presented in Table 1. The broadening increases significantly with La^{3+} substitution. It is well accepted that the broadness in relaxor originates from the compositional fluctuation and disorder in crystallographic sites when one or more cations occupy the same site in the structure [38]. La^{3+} exaggerates the compositional fluctuation in BBT. As a result broadness increases.

Fig. 5 shows the temperature dependence of permittivity for $x = 0.1$ and $x = 0.5$ at different frequencies. A significant frequency dispersion of permittivity is observed with increasing substitution. This indicates the substitution enhances relaxor behaviour in BBT. Similar relaxor behaviour is observed for grain oriented $BaBi_2Nb_2O_9$ ceramics [39].

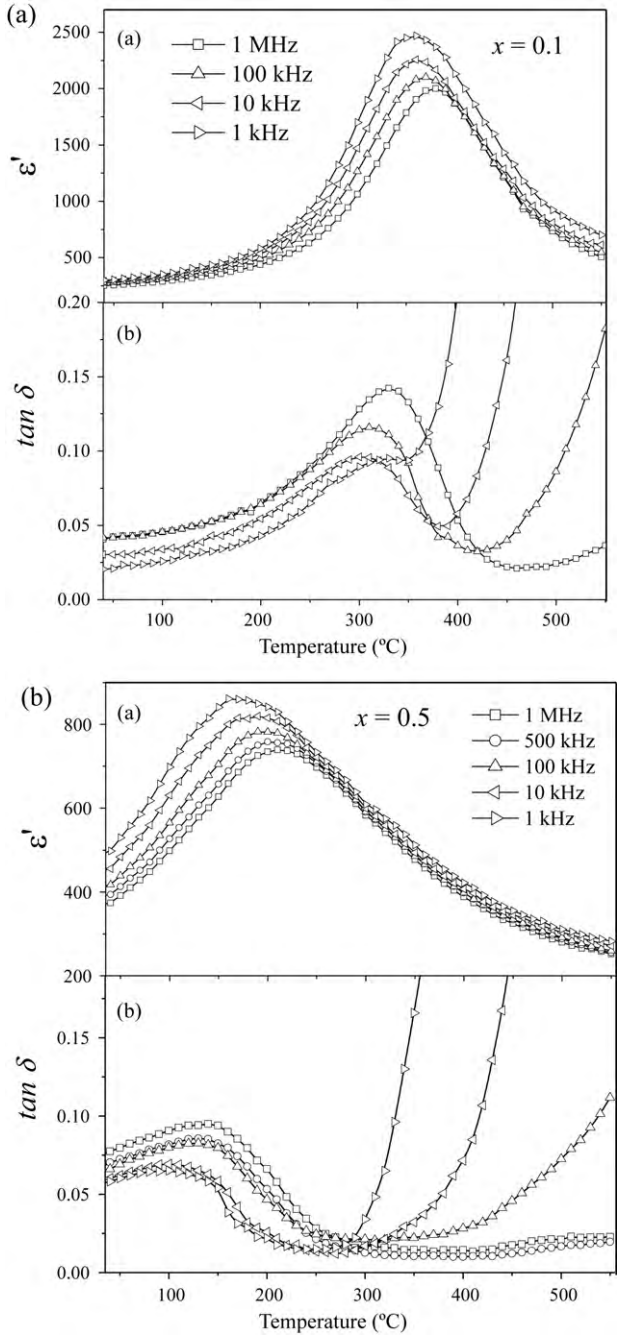

Fig. 5. Temperature dependence of ε' and $\tan\delta$ at various frequencies for $BaBi_{(4-x)}La_xTi_4O_{15}$ ceramics (a) $x = 0.1$ and (b) $x = 0.5$.

The diffusivity (γ) parameter is applied to characterize the relaxor behaviour and it is expressed by a modified Curie–Weiss law [40]:

$$\frac{1}{\varepsilon'} - \frac{1}{\varepsilon_{m'}} = \frac{(T - T_m)^{\gamma}}{C_1} \tag{4}$$

where $\varepsilon_{m'}$ is the maximum dielectric constant, γ is the degree of diffuseness and C_1 is a constant. The values of γ lie in the range 1–2. In case of ideal ferroelectrics, $\gamma = 1$ and for ideal relaxors, $\gamma = 2$. Fig. 6 shows the plot of $\log(1/\varepsilon' - 1/\varepsilon_{m'})$ versus $\log(T - T_m)$ and calculated γ values for different compositions. It is evident that γ increases with increase in La^{3+}. That is the degree of diffuseness or relaxor behaviour increased with La^{3+} substitution.

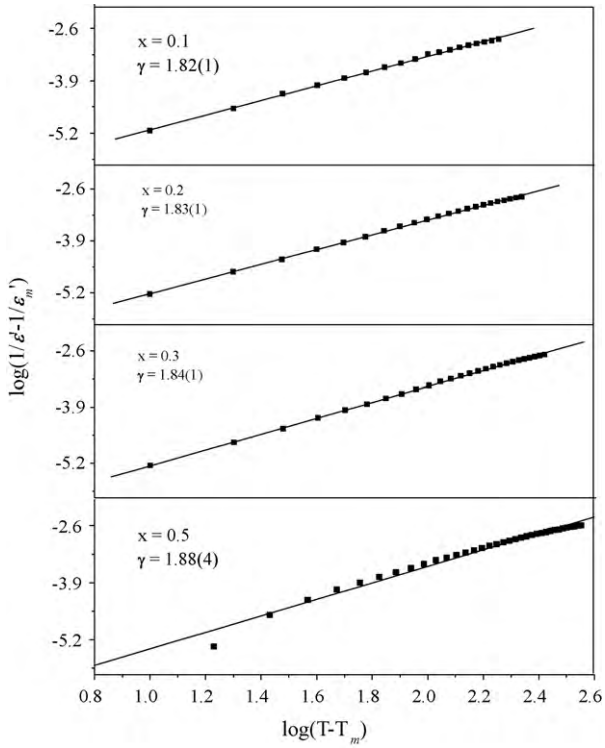

Fig. 6. Plot of $\log(1/\varepsilon' - 1/\varepsilon_{m'})$ versus $\log(T - T_m)$ for different $BaBi_{(4-x)}La_xTi_4O_{15}$ ($x = 0.1, 0.2, 0.3, 0.5$) ceramics.

The frequency dispersion in relaxor may be described as [41]:

$$\Delta T_m = T\varepsilon_{m(1\,MHz)'} - T\varepsilon_{m(1\,kHz)'} \tag{5}$$

where $T\varepsilon_{m'(1\,MHz)}$ and $T\varepsilon_{m'(1\,kHz)}$ is the maximum permittivity temperature at 1 MHz and 1 kHz, respectively. ΔT_m of different compositions are listed in Table 1. ΔT_m increases from 20 °C (for BBLT1) to 50 °C (for BBLT5). The result indicates the substitution enhances frequency dispersion or relaxor behaviour.

In relaxor ferroelectrics, dielectric relaxation is expressed by Vogel–Fulcher relationship [42]:

$$\nu = \nu_0 \exp\left\{\frac{-E_a}{k_B(T_m - T_f)}\right\} \tag{6}$$

where ν_0 is the attempt frequency of dipole reorientation, E_a is the activation energy (i.e., the energy barrier between two equivalent polarization states), k_B is the Boltzmann's constant, T_f is the static freezing temperature (i.e., the temperature at which dynamic reorientation of the dipolar cluster polarization can no longer be thermally activated). Fig. 7 shows the plot of $1/T_m$ versus $\log\nu$ for $x = 0.1$–0.5 compositions. Open symbols represent the experimental data points and the line gives the fit to Eq. (6). The T_m shows a good fit to Vogel–Fulcher law and confirms them to possess relaxor characteristics. The values for fitting parameters ν_0, E_a and T_f are listed in Table 1. The E_a increases with increase in La^{3+} concentration confirming the strengthening in the relaxation behaviour [13]. As stated above, E_a represents the energy barrier between two equivalent polarization states under *AC* field. As energy increases, polarization becomes more dependent on frequency, which is one of the major characteristics of relaxor. The static freezing temperature is also found to decrease with increasing La^{3+} substitution.

3.4. Ferroelectric polarization versus electric field study

Fig. 8 shows the ferroelectric hysteresis loop of $BaBi_{(4-x)}La_xTi_4O_{15}$ ceramics obtained under a maximum applied

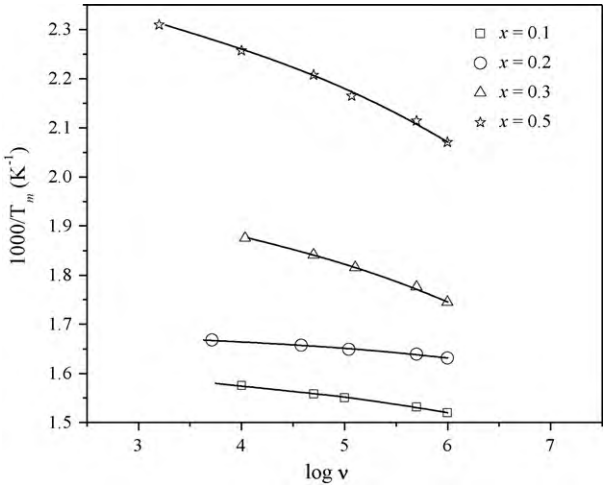

Fig. 7. Frequency dependence of T_m. The symbols and solid line indicate data points and fit to Vogel–Fulcher relationship, respectively.

electric field of 30 kV cm^{-1}. Though the loops are far from saturation due to the limitation of the experimental setup, the data can still be used for comparison purpose as they are taken at the same electric field for different compositions. This can provide an overview on the variation of remnant polarization and coercive field with La^{3+} substitution. The *P–E* loop for all the compositions are recorded at room temperature and at a frequency of 100 Hz. The values of remnant polarization ($2P_r$) and coercive field ($2E_c$) are listed in Table 1. With La^{3+} substitution, $2P_r$ increases up to $x = 0.3$. BBLT3 showed highest $2P_r$ among all and a lower $2E_c$ than BBT [43].

The initial increase in $2P_r$ may be due to the decrease in concentration of oxygen vacancies in the system. As a result, the domain pinning effect gets decreased, enhancing $2P_r$. In general, the Bi_2O_2 layers of BLSF plays the role of an insulating layer by compensating the space charge effect and also refrains the oxygen vacancies from accumulating at the domain walls, thus pinning the domains [1]. With increase in La^{3+} substitution, the La^{3+} ions get incorporated in the Bi_2O_2 layers. Thus, role of Bi_2O_2 layer is weakened and it is unable to prevent the collection of oxygen vacancies at domain walls, thus resulting in a decreased $2P_r$.

3.5. dc-conductivity

Cole–Cole plots obtained from impedance spectra are shown in Fig. 9. To extract resistance (*R*) and capacitance (*C*) values, an equivalent circuit comprising of two parallel resistor–capacitor (*RC*) elements connected in series is used to model the electrical response of grain and grain-boundary regions. *R* and *C* are determined from Cole–Cole plot using ZView software. At high temperatures from ~450 °C, two semicircles could be traced. The

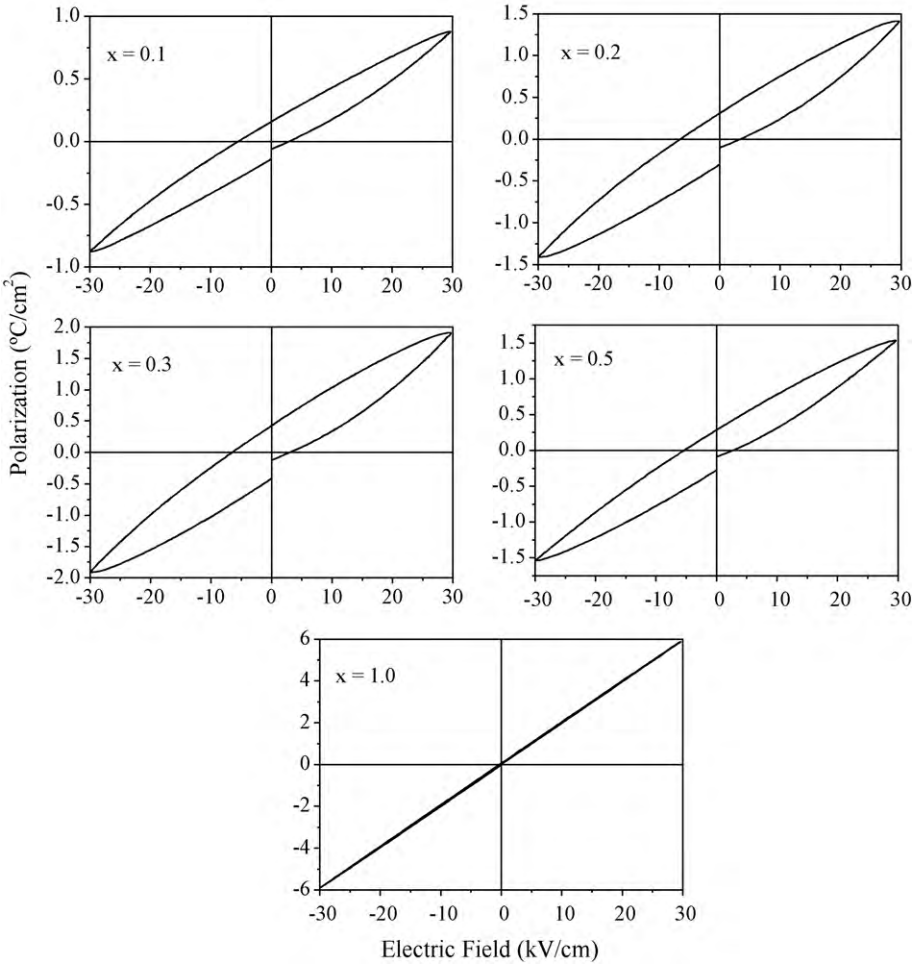

Fig. 8. Plot of ferroelectric hysteresis loop measured at room temperature for different $BaBi_{(4-x)}La_xTi_4O_{15}$ ($x = 0.1, 0.2, 0.3, 0.5$) ceramics.

Table 2
Activation energy for grain (E_g) and grain-boundary (E_{gb}), dc-conductivity for grain and grain boundary at 550 °C for different $BaBi_{(4-x)}La_xTi_4O_{15}$ ceramics.

Formula	BBLT1	BBLT2	BBLT3	BBLT5	BBLT10
E_g (eV)	0.218	0.273	0.355	0.213	0.261
E_{gb} (eV)	0.416	0.545	0.672	0.238	0.549
σ_{dc} (Ω^{-1} cm^{-1}) (grains)	2.9×10^{-6}	7.41×10^{-7}	2.77×10^{-7}	9.8×10^{-7}	6.48×10^{-7}
σ_{dc} (Ω^{-1} cm^{-1}) (grain boundary)	2.4×10^{-6}	6.92×10^{-7}	2.46×10^{-7}	9.33×10^{-7}	6.07×10^{-7}

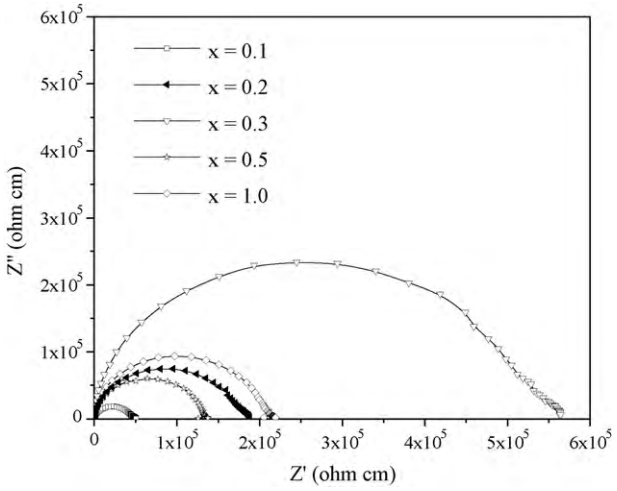

Fig. 9. Complex impedance plots of $BaBi_{(4-x)}La_xTi_4O_{15}$ ($x = 0.1, 0.2, 0.3, 0.5$) ceramics at 550 °C.

intercepts of the high frequency and low frequency arc give the grain resistance (R_g) and grain-boundary resistance (R_{gb}), respectively. Respective capacitances can be calculated using the relation $2\pi f_m RC = 1$, where f_m is the maximum frequency of the semicircle. Using the above R values, the dc conductivities of grain and grain-boundary regions can be evaluated using the relation,

$$\sigma_{dc} = \frac{d}{RA} \tag{7}$$

where d is the thickness of the pellet, A is the electrode area and R is the grain or grain-boundary resistance. R is derived by fitting the complex impedance data to the equivalent circuit model as described above. Grain and grain-boundary dc-conductivity at 550 °C are listed in Table 2. Conductivity decreases with substitution due to the same reason of decreased oxygen vacancies.

The composition with $x = 0.3$ show lowest dc-conductivity among all. The activation energy for grain (E_g) and grain-boundary (E_{gb}) regions are calculated from the temperature dependence of the dc-conductivity using the Arrhenius relation:

$$\sigma = \sigma_o \exp\left(\frac{-E_a}{k_B T}\right) \tag{8}$$

where σ_o is the pre-exponential factor, k_B is the Boltzmann constant and T is the absolute temperature. The values of E_g and E_{gb} are listed in Table 2. E_{gb} is higher than E_g, due to more resistive grain boundaries compared to grains. Grain boundaries are more resistive as they are easily oxidized during the cooling step of sintering

4. Conclusion

La^{3+} substitution for Bi^{3+} in $BaBi_4Ti_4O_{15}$ ceramics significantly affects the dielectric properties. The single-phase $BaBi_{4-x}La_xTi_4O_{15}$ solid solution is observed for $x \leq 1.0$. The grain size is suppressed in doped samples. The temperature of the dielectric maximum is lowered and the dielectric loss decreases with La^{3+} substitution. The diffuseness and relaxor behaviour are found to increase with increasing x. The increase in the relaxor behaviour can probably be attributed to the compositional fluctuation induced by La^{3+}, partly in perovskite and partly in Bi_2O_2 layers. The dielectric relaxations show a sufficiently good fit with the Vogel–Fulcher relationship. The freezing temperature T_f is noted to decrease from 310 to 100 °C with increasing x from 0.1 to 0.5. BBLT3 showed highest $2P_r$ among all and a lower $2E_c$ than BBT. The incorporation of La^{3+} ions also results in a significant reduction in the dc-conductivity in $x = 0.3$ composition. The increased activation energies and decreased dc conductivities confirms the decrease in oxygen vacancy concentration with La^{3+} substitution.

Acknowledgment

The University Grants Commission, Government of India, is gratefully acknowledged for financial support to this research work.

References

[1] C.A.P. de Araujo, J.D. Cuchiaro, L.D. McMillan, M. Scott, J.F. Scott, Nature 374 (1995) 627–629.
[2] B.H. Park, B.S. Kang, S.D. Bu, T.W. Noh, J. Lee, W. Jo, Nature 40 (1999) 682–684.
[3] H. Yan, H. Zang, M.J. Reece, X. Dong, Appl. Phys. Lett. 87 (2005) 082911–082913.
[4] B. Yang, F. Wang, J. Han, Y. Chen, S. Zhu, Z. Liu, W. Cao, Thin Solid Films 473 (2005) 296–299.
[5] H. Du, W. Zhou, F. Luo, D. Zhu, S. Qu, Z. Pei, Appl. Phys. Lett. 91 (2007) 182909–182911.
[6] B. Aurivillius, Ark. Kemi. 1 (1949) 463–480.
[7] R.L. Withers, J.G. Thompson, A.D. Rae, J. Solid State Chem. 94 (1991) 404–417.
[8] A.D. Rae, J.G. Thompson, R.L. Withers, Acta Crystallogr. B 48 (1992) 418–428.
[9] R.Z. Hou, X.M. Chen, Y.W. Zeng, J. Am. Ceram. Soc. 89 (2006) 2839–2844.
[10] I. Pribosic, D. Makovec, M. Drofenik, J. Eur. Ceram. Soc. 21 (2001) 1327–1331.
[11] T. Kobayashi, Y. Noguchi, M. Miyayama, Appl. Phys. Lett. 86 (2005) 012907–012909.
[12] D. Makovec, I. Pribosic, Z. Samardzija, M. Drofenik, J. Am. Ceram. Soc. 84 (2001) 2702–2704.
[13] S. Kumar, K.B.R. Varma, J. Phys. D: Appl. Phys. 42 (2009) 075405–075414.
[14] A. Snedden, S.M. Blake, P. Lightfoot, Solid State Ionics 156 (2003) 439–445.
[15] A. Chakrabarti, J. Bera, Curr. Appl. Phys. 10 (2010) 574–579.
[16] S. Huang, C. Feng, M. Gu, Y. Li, J. Alloys Compd. 472 (2009) 262–266.
[17] Z. Zhou, X. Dong, S. Huang, J. Am. Ceram. Soc. 89 (2006) 2939–2942.
[18] R.Z. Hou, X.M. Chen, Mater. Res. Bull. 38 (2003) 38–63.
[19] R.Z. Hou, X.M. Chen, Solid State Commun. 130 (2004) 469–472.
[20] S. Rachna, S. Bhattacharyya, S.M. Gupta, J. Phys. Chem. Solids 69 (2008) 822–829.
[21] V.B. Santos, J.-C. M'Peko, M. Mir, V.R. Mastelaro, A.C. Hernandes, J. Eur. Ceram. Soc. 29 (2009) 751–756.
[22] X.B. Chen, R. Hui, J. Zhu, W.P. Lu, X.Y. Mao, J. Appl. Phys. 96 (2004) 5697–5700.
[23] H. Sun, X.B. Chen, J. Zhu, J.H. He, Y.F. Qian, H. Fang, J. Sol–Gel Sci. Technol. 43 (2007) 125–129.
[24] A.Z. Simoes, C.S. Riccardi, F. Moura, A. Ries, N.L.A. Junior, M.A. Zaghete, B. Stojanovic, E. Longo, J.A. Varela, Mater. Lett. 58 (2004) 2842–2847.
[25] Y.Y. Yao, C.H. Song, P. Bao, D. Su, X.M. Lu, J.S. Zhu, Y.N. Wang, J. Appl. Phys. 95 (2004) 3126–3131.
[26] M. Shimazu, J. Tanaka, K. Muramatsu, M. Tsukioka, J. Solid State Chem. 35 (1980) 402–406.
[27] A. Chakrabarti, J. Bera, T.P. Sinha, Physica B 404 (2009) 1498–1502.
[28] S.M. Huang, C.D. Feng, L.D. Chen, X.W. Wen, Solid State Commun. 133 (2005) 375–379.
[29] http://www.ing.unitn.it/~maud.
[30] J. Arreguin-Zavala, M.E. Villafuerte-Castrejon, F. Gonzalez, L. Bucio, O. Novelo-Peralta, R.Y. Sato-Berru, J. Ocotlan-Flores, Mater. Charact. 60 (2009) 219–224.
[31] A. Husur, J.H. Ko, S. Kojima, S.S. Lee, M.S. Jang, J. Korean Phys. Soc. 41 (2002) 763–768.
[32] F. Suhua, Z. Fengqing, W. Peiji, R. Yanxia, J. Rare Earths 26 (2008) 575–578.
[33] Y. Shimakawa, Y. Kubo, Y. Tauchi, H. Asano, T. Kamiyama, F. Izumi, Z. Hiroi, Appl. Phys. Lett. 79 (2001) 2791–2793.

[34] K.R. Kendall, C. Navas, J.K. Thomas, H.-C. Zur Loye, Chem. Mater. 8 (1996) 642–649.
[35] E.C. Subbarao, J. Phys. Chem. Solids 23 (1962) 665–676.
[36] D.Y. Saurez, I.M. Reaney, W.E. Lee, J. Mater. Res. 11 (2001) 3139–3149.
[37] V.V. Kirillov, V.A. Isupov, Ferroelectrics 5 (1973) 3–9.
[38] J. Tellier, Ph. Boullay, M. Manier, D. Mercurio, J. Solid State Chem. 177 (2004) 1829–1837.
[39] H.X Yan, H.T. Zhang, R. Ubic, M. Reece, J. Liu, Z. Shen, J. Mater. Sci. Mater. Electron. 17 (2006) 657–661.
[40] K. Uchino, S. Nomura, Ferroelectrics 44 (1982) 55–61.
[41] X.W. Zhang, F. Fang, J. Mater. Res. 14 (1999) 4581–4586.
[42] D. Viehland, S.J. Jang, L.E. Cross, J. Appl. Phys. 68 (1990) 2916–2921.
[43] A.V. Murugan, S.C. Navale, V. Ravi, Mater. Lett. 60 (2006) 1023–1025.